Cancer Research

CUL3 and NRF2 mutations confer an NRF2 activation phenotype in a sporadic form of papillary renal cell carcinoma

Aikseng Ooi, Karl Dykema, Asif Ansari, et al.

Cancer Res Published OnlineFirst January 30, 2013.

Title

CUL3 and *NRF2* mutations confer an NRF2 activation phenotype in a sporadic form of papillary renal cell carcinoma

Authors

[1†]Aikseng Ooi, Ph.D.

[1]Karl Dykema

[2]Asif Ansari, M.D.

[1]David Petillo, Ph.D.

[1]John Snider

[2]Richard Kahnoski, M.D.

[2]John Anema, M.D.

[3]David Craig, Ph.D.

[3]John Carpten, Ph.D.

[4,5,6]Bin-Tean Teh, M.D., Ph.D.

[1†]Kyle A. Furge, Ph.D.

Affiliations

1. Interdisciplinary Renal Oncology Laboratory, Van Andel Research Institute, Grand Rapids, MI, 49503 USA
2. Spectrum Health, Grand Rapids, MI, 49503 USA
3. Translational Genomics Research Institute, Phoenix, AZ 85004 USA
4. NCCS-VARI Translational Cancer Research Laboratory, National Cancer Centre of Singapore

5. Singhealth, Singapore General Hospital

6. Duke-NUS, Singapore

Contact[†]

Kyle A. Furge

e-mail: kyle.furge@vai.org

Aikseng Ooi

e-mail: aikseng.ooi@vai.org

Running Title

Somatic mutations activate NRF2 in kidney cancer

Disclosure of Potential Conflicts of Interest

The authors declare no potential conflicts of interest.

Author's contributions

Conception and design: A. Ooi, K. Furge

Development of methodology: A. Ooi

Acquisition of data (provided animals, acquired and managed patients, provided facilities, etc.): A. Ooi, A. Ansari, D. Petillo, J. Snider, R. Kahnoski, J. Anema, J. Carpten, D. Craig, B.T. Teh

Analysis and interpretation of data (e.g., statistical analysis, biostatistics, computational analysis): A. Ooi, K. Dykema

Writing, review, and/or revision of the manuscript: A. Ooi, K. Furge

Administrative, technical, or material support (i.e., reporting or organizing data, constructing databases): A. Ooi, D. Petillo, J. Snider, A. Ansari, K. Dykema, K. Furge

Study supervision: K. Furge

Grant Support

This work was funded by the Van Andel Research Institute.

Abstract

Sustained activation of the stress-regulated transcription factor NRF2 (NFE2L2) is a prominent feature of many types of cancer, implying that mutations driving NRF2 may be important to tumor progression. In hereditary type 2 papillary renal cell carcinoma (PRCC2, also known as hereditary leiomyomatosis and renal cell cancer, HLRCC), NRF2 activation is a direct consequence of the accumulation of intracellular fumarate, a result of fumarate hydratase (FH) inactivation, but it is not clear how NRF2 may be activated in sporadic forms of PRCC2. Here we show that somatic mutations in *NRF2*, *CUL3,* and *SIRT1* are responsible for driving the NRF2 activation phenotype in sporadic PRCC2. Transcriptome sequencing revealed the expression pattern of mutant alleles of *NRF2*, *CUL3*, and *SIRT1* and also confirmed NRF2 activation in clinical specimens. Our results demonstrate a convergence in somatic mutations in sporadic PRCC2 with FH mutation in hereditary PRCC2.

Introduction

Nuclear factor [erythroid-derived 2]-like 2 (NRF2) transcription factor regulates the transcription of a large number of genes that constitute biochemical pathways including xenobiotic metabolism, energy metabolism, and cell cycle regulation. Its activity is largely regulated by Kelch-like ECH-associated protein 1 (KEAP1), which acts as an adaptor protein that facilitates NRF2 ubiquitination and subsequent degradation. Gain-of-function mutation to *NRF2* and loss-of-function mutation to *KEAP1* have been found in a large number of tumors (1-3). Because both of these mutations cause sustained NRF2 activation, it is likely that such activation is important to tumor progression.

Type 2 papillary renal cell carcinoma (PRCC2) is a kidney cancer subtype that has a high mortality rate. Individuals who inherit a germline mutation in the fumarate hydratase (*FH*) gene are predisposed to developing PRCC2 (4). Sporadic cases of PRCC2 rarely harbor an *FH* mutation, and the driver mutations in these tumors remain unknown (5). Despite differences in genetic etiology, both forms of PRCC2 share many clinical and morphological phenotypes. The most prominent shared biochemical feature is sustained activation of the NRF2 (6). NRF2 activation in hereditary PRCC2 is caused by the accumulation of intracellular fumarate, which is a result of FH inactivation (6); the mechanism of NRF2 activation in sporadic PRCC2 has yet to be determined. We hypothesized that NRF2 activation in sporadic PRCC2 is caused by somatic mutation to genes that directly regulate NRF2 transcription activity.

Materials and Methods

Cell line

Primary human normal renal proximal tubule epithelial cells, PCS-400, were purchased from ATCC in year 2012. Each batch of the primary cell line was authenticated by ATCC for the presence of γ-glutamyl transferase activity, a marker for renal proximal tubule epithelial cells. Cells also tested negative for hepatitis C, HIV (human immunodeficiency virus), bacteria and mycoplasma. Cells from the third passage were used in this study.

Clinical samples

Four of the five clinical samples were acquired through the Cooperative Human Tissue Network, and one was acquired from Spectrum Health Hospital, Grand Rapids, Michigan, USA. The Van Andel Institute and Spectrum Health Institutional Review Boards approved the study protocols, and all patients signed a written consent form.

Massively parallel sequencing

Total genomic DNA was isolated from cryosections of fresh-frozen tissues using a phenol/chloroform/isopropanol method. The coding exons of the indicated samples were isolated using the Agilent SureSelect All Exon 50Mb Kit, following the manufacturer's recommended protocols. DNA sequencing was performed using an Illumina HiSEQ. Raw sequencing reads were filtered to remove duplicate reads using Picard Tools 1.29 and were aligned to the reference genome (hg18) using BWA v0.5.8a (7, 8). Variants that differed between tumor and normal samples were identified using SomaticSniper 1.0.0 and annotated using SeattleSeq Annotation server (9). Total RNA was isolated using TRIzol® (Invitrogen) reagent and sequenced using the Illumina HiSEQ following manufacturers' protocols. The raw sequencing reads were mapped to the reference genome (hg18) using Tophat v1.3.3 (10). Location-specific sequence extraction and examination were done using SAMTools (11). Small insertions and deletions (indels) that a) occurred within coding exons, b) had associated quality scores greater than 900, c) had read depths greater than 100, and d) were not present in associated normal samples using the same filtering criteria were identified using the GATK unified genotyper (GenomeAnalysisTK-1.2-58-gc1329c4) and vcftools_0.1.9 (12). The mapped reads for both exome and transcriptome sequencing have been deposited in the Gene Expression Omnibus (GEO) database.

Statistical analyses

Statistical analyses were performed using the R statistical environment (Version 2.14.0, x86_64-apple-darwin9.8.0/x86_64 [64-bit]) (13). Wherever applicable, computation was accelerated using the "Multicore" package (14). Differential gene expression analysis on transcriptome sequencing data was performed using the DESeq package (15). Total read counts covering each exon were extracted using SAMTools and were used in the differential gene expression analysis. Gene-specific Fragments Per Kilobase of exon per Million fragments mapped (FPKM) values were calculated using Cufflinks (16). Expression data were pre-filtered to exclude non-informative features before statistical analysis; features having values less than the first quartile of the overall data in greater than 75% of the samples were deem non-informative. All p-values from statistical significance tests were adjusted for false discovery rate (fdr) using methods described by Benjamini and Hochberg (1995) (17).

Expression constructs

Expression plasmid constructs carrying variants of the wild-type genes in this study have been published by others and made available through Addgene. These plasmids were pcDNA3-HA2-KEAP1(18), pCDNA3-Myc3-Nrf2 (18), and pECE-Flag-SIRT1 (19). Mutant variants were created through PCR-mediated site-directed mutagenesis. The reporter constructs pRL-CMV and pGL4-Luc2P-NRF2-RE-Hygro were purchased from Promega. Reporter assays using these clones were performed using the DualGlo-Luciferase Reporter Assay System (Promega) according to the manufacturer's

recommended protocols. RNA interference-mediated knockdown of *CUL3* was performed using two species of siRNA with sequences GGAUCGCAAAGUAUACACAUAUGUA and UACAUAUGUGUAUACUUUGCGAUCC (Invitrogen). The 3xflag-tagged versions of wild-type NRF2, the E82G mutant, and the V36 deletion mutant constructs were also created on the pIRESPuro plasmid backbone (Clonetech).

Cycloheximide chase experiment

A cycloheximide (CHX) chase experiment was performed by transfecting PCS-400 cells with the 3xflag-tagged version of wild-type NRF2, of the E82G mutant, or of the V36 deletion mutant. At 24 h post-transfection, cells were split into six separate 6-well cell culture dishes and maintain for another 24 h. After that, cell culture medium in all cell culture dishes were replaced with fresh warm medium containing 100 μg/ml of CHX. Protein lysate was isolated at a 25-min interval for six continuous time points. NRF2 protein levels were detected by western blot using an anti-DYKDDDDK tag antibody (Cell Signaling Technology). Relative protein abundance was estimated using a densitometry method (ImageJ). Loading variation was cancelled out by dividing the estimated NRF2 protein density with its corresponding actin protein density. Dividing protein density of each time point by the relative density of time zero give the sample-specific normalization. For NRF2-WT and NRF2-E82G, which follow regular exponential decay, half-life ($t_{1/2}$) was estimated using the equation of exponential decay: $\ln 2/\lambda = t_{1/2}$. Constant λ was estimated by fitting the data onto exponential decay function: $N = N_o\, e^{-\lambda t}$, where N_o is protein abundance at time zero and N is apparent protein

abundance. For NRF2-E82G, which follows a logistic decay function, inflection point (t_i) was estimated according to $N = a/(1+e^{((ti-t)/b)})$, where a is the asymptote, b is a numerical scale constant, and e is the Euler number.

Immunohistochemistry staining of NRF2 on clinical samples

The NRF2 protein level in the formalin-fixed paraffin-embedded tissue samples was detected by immunohistochemical staining using an anti-human-NRF2 rabbit polyclonal antibody (ab31163, Abcam) at a dilution of 1:500. The staining was performed using EnVision™ + staining kit (Dako) according to the manufacturer's recommended protocol. Antigen retrieval was performed by autoclaving the slides (121 ^{o}C, 15-16 psi, 15 min) in Target Retrieval Solution (Dako).

Accession numbers

The exome sequencing data generated in this study have been deposited into the Sequence Read Archive of the European Bioinformatics Institute (EBI). The data accession number is ERP002035. The transcriptome sequencing data generated in this study have been deposited into the Sequence Read Archive of the National Center for Biotechnology Information (NCBI). The data accession number is SRP015003.

Results

Somatic mutations to *NRF2*, *CUL3*, and *SIRT1* are found in sporadic PRCC2

Many of the current efforts in identifying driver mutations rely on the sequencing of a large number of cancers of a defined subtype to identify somatic mutations that occur

more frequently than expected by chance alone (20). The incidence of PRCC2 in the general population is relatively low; consequently collecting large sample size translates into increased cancer-related deaths. To overcome this, we devised a knowledge-guided strategy of driver mutation discovery. We considered that some of the driver mutations in sporadic PRCC2 cause sustained NRF2 activation, because both hereditary and sporadic PRCC2 converge at this biochemical phenotype. Consequently, assessing the effect of mutants on NRF2 activity could identify driver mutations. Specifically, we mined scientific literature databases to construct an NRF2 regulatory pathway (Figure S1), which we subsequently used to screen non-synonymous mutation calls from exome-captured massively parallel sequencing (exome sequencing).

We performed exome sequencing on matched tumor vs. normal samples from five cases of confirmed sporadic PRCC2, that identified 3318 somatic mutations that involved 1614 known genes (Table S1). The initial screening identified mutations in three different genes. These gene mutations could account for NRF2 activation in four of the five cases of PRCC2. Potential gain-of-function *NRF2* mutations were found in two cases: Case-831 contained a c.245A>G transition resulting in a change of glutamate 82 to glycine (E82G), and Case-666 contained a c.105_107delGTA deletion causing loss of valine 36 (Figures 1A and B). Case-666 also had a *SIRT1* c.808T>C transition, which changed isoleucine 270 to threonine (I270T; Figure 1B**).** Two of the remaining cases contained *CUL3* mutations, Case-337 with a c.1168delT deletion and Case-790 with a c.2125C>T transition, which result, respectively, in a frame shift (L390fs) and a change of arginine

708 to tryptophan (R708W) (Figures 1C and D). These somatic mutations were confirmed by dideoxynucleotide sequencing (Figure S2).

The identified somatic mutations render NRF2 insensitive to KEAP1-mediated degradation

The functional consequences of the mutations we identified could be deduced from prior knowledge of how protein levels and transcriptional activity of NRF2 are regulated. NRF2 consists of six highly conserved Nrf2-ECH homology (Neh) domains (21). Contained within the Neh2 domain are two conserved motifs, DIDLID and ETGE, which are required for efficient binding with KEAP1 through interaction with its Kelch-repeat domain (21, 22). Under homeostatic conditions, NRF2 binds to KEAP1, which is tethered to the cytosol and brings NRF2 into close proximity with CUL3 ubiquitin ligase (23). NRF2 is then ubiquitinated by the KEAP1-CUL3 complex and degraded through a proteasome-mediated degradation pathway.

KEAP1 acts as cellular oxidative sensor: thiol-reactive compounds can react with its surface cysteine residues, causing it to undergo a conformational change that renders it unable to bind NRF2. Loss of the KEAP1-CUL3-NRF2 interaction results in NRF2 accumulation and thus increased expression of NRF2 transcriptional targets (6, 24). The c.245A>G mutation that results in the E82G substitution directly affects the ETGE motif within the Neh2 domain, altering the sequence to ETGG. The c.105_107delGTA deletion removes valine 36, which resides within the Neh2 domain between the DIDLID

and ETGE motifs. This mutation does not change the DIDLID or ETGE motifs but shortens the distance between them.

To determine whether the *NRF2* mutations resulted in NRF2 transcriptional activity that is insensitive to KEAP1-mediated regulation, we ectopically expressed the wild-type and the E82G forms of NRF2 in a primary kidney tubular epithelial cell line (PCS-400), with and without the present of ectopically expressed, HA-tagged KEAP1. NRF2 transcriptional activity was followed using a firefly luciferase reporter controlled by a 3-tandem antioxidant response element (ARE) enhancer sequence that was cloned in front of a basic promoter on a pGL4-based vector (Promega) (Figure S3). As expected, the E82G mutation produced NRF2 mutant proteins more stable toward KEAP1-mediated degradation, while the transcriptional activity remained unchanged even with co-expression of exogenous KEAP1 (Figure 2A). These results suggest that the mutation stabilizes NRF2 by disrupting its ability to bind to KEAP1. We performed similar assays on the transcriptional activity of the *NRF2* c.105_107delGTA deletion mutant (denoted as NRF2 V36del). Our results suggest that the mutation produced an NRF2 molecule that was stable even with ectopic expression of *KEAP1* (Figure 2B). A subsequent CHX chase experiment confirmed that both NRF2 E82G and NRF2 V36del are more stable than the wild-type NRF2 (Figure S4).

NRF2 is also regulated by an acetylation/deacetylation cycle mediated by the cAMP response element binding protein (CBP) and SIRT1 (25). Acetylation of NRF2 by CBP increases its nuclear localization and transcriptional activity, and this modification is

reversed by SIRT1-mediated deacetylation. Mutations have been identified in SIRT1 that function as dominant negatives by disrupting the deacetylase activity. Specifically, expression of SIRT1 protein that contains an H355A mutation increases the transcriptional activity of NRF2 (25). We found the I270T *SIRT1* mutation in the same sample as the *NRF2* c.105_107delGTA mutation. Expression of the I270T mutant has a small effect on the transcriptional activity of NRF2 c.105_107delGTA mutant gene product. Specifically, it enhanced the transcriptional activity of NRF2 to the level of the E82G mutant (Figures 2A and B). Since CUL3 is the ubiquitin ligase that marks NRF2 for proteasomal degradation, a loss of CUL3 function could increase NRF2 activity, which has been previously demonstrated by Liognon and co-workers in breast cancer tissues (26). One of the two *CUL3* mutations was a deletion that causes a frame shift and complete loss of CUL3 function. We used siRNA-mediated knockdown of endogenous CUL3 to approximate the frameshift event. As expected, the transient knockdown of CUL3 resulted in higher NRF2 activity (Figure 2C), supporting our hypothesis that the *CUL3* mutations are the driver of NRF2 activation phenotype in two of the five cases of sporadic PRCC2. We were not able to identify a mutation that could drive NRF2 activation in one of the five samples sequenced. This suggests either a knowledge gap in the regulation of NRF2 transcriptional activity or an epigenetic event that was not captured by the exome sequencing.

Effects of the identified mutations on the transcriptome

We performed transcriptome sequencing on the same five cases of sporadic PRCC2 to investigate the effect of NRF2 activation and the expression of the mutant alleles that

disrupted NRF2 regulation. As expected, the transcript levels of many known transcription targets of NRF2—including *AKR1C3* (aldo-keto reductase family 1 member C3),(27) *AKR1C1* (aldo-keto reductase family 1 member C1),(27) *AKR1B10* (aldo-keto reductase family 1 member B10) (6, 27), *NQO1* (NAD[P]H:quinone oxidoreductase)(28), and *TXNRD1* (thioredoxin reductase 1) (29)—were significantly higher in the tumor samples than in matched adjacent control samples, indicating the sequenced tumor samples were indeed exhibiting an NRF2 activation phenotype (Figure 3A, Table S2). Subsequent immunohistochemical staining for NRF2 protein in those samples also showed intense positive nuclear staining (Figure 3B). At the same time, normal kidney and clear cell renal cell carcinoma tissues showed negative staining (Figure 3C, 3D). Hence the results support our deduction that NRF2 was indeed activated in these tissues. Also, the non-frame-shift mutant alleles were transcribed in the corresponding samples (Figures 4A-C). However, the transcript of the *CUL3* c.1168delT mutation was not present in the transcriptome sequencing data (Figure 4D). The absence of the frameshift transcript suggests possible nonsense-mediated decay.

Discussion

Despite being an aggressive cancer, PRCC2 remains largely understudied. Much of our understanding in PRCC2 come from studying hereditary form of the tumor which arise in patient with hereditary leiomyomatosis and renal cell cancer (HLRCC) syndrome. Ever since the discovery of the association between *FH* mutation and HLRCC, studies on the hereditary form of PRCC2 have been focusing on the activation of the hypoxia inducible factor 1 alpha (HIF1A). We recently discovered that in NRF2 is activated in hereditary

PRCC2 tissues, and it is a direct consequence of FH inactivation (6). Specifically, fumarate, which accumulates as a result of FH inactivation, covalently modifies KEAP1 and renders it unable to bind NRF2, leading to NRF2 activation (6). A separate study using an *Fh-Hif1a* double knockout mouse showed that the knocking out *Hif1a* against the background of the *Fh* knockout exacerbated the disease phenotype, providing evidence that the *Hif1a* could be a compensatory event (30). Further, the expression profile of the diseased tissue derived from the *Fh* knockout and the *Fh-Hif1a* double knockout were very similar. Notably, the overexpression of pro-glycolytic genes—such as *Slc2A1* (glucose transporter 1) and *PKM2* (pyruvate kinase)—that was thought to be the result of *Hif1a* activation, remained unchanged in the *Fh-Hif1a* double knockout (31).

Results from this study and others have shown that NRF2 activation is positively selected in tumors, suggesting that it contributes to tumorigenesis. For instance, NRF2 activation is a known feature of a large fraction of lung cancers. The NRF2 activation phenotype is known to result from *NRF2* gain-of-function and *KEAP1* loss-of-function mutations (1). We also found that a subset of lung cancers harbor *CUL3* mutations, and the transcription profiles from these cases mirror those with NRF2 activation (results not shown). NRF2 activation has been reported to be a consequence of oncogene activation, suggesting that NRF2 could be the downstream effector that is responsible for tumorigenesis (32). Ectopic expression of constitutively active NRF2 has been shown to confer tumorigenic potential (33), although the mechanism for NRF2 conferring such potential is unknown.

Paradoxically, NRF2 modulates the expression of many genes involved in xenobiotic metabolism and neutralization of reactive oxygen species. NRF2 activation is believed to be the mechanism of tumor suppressive effects of many compounds, as well as caloric restriction (34, 35). These contradictory effects of NRF2 activation could be partly explained by the variability that exists in the regulatory effect of NRF2 on its transcription targets. The availability of NRF2 targets can be affected by the activity of chromatin modifiers such as BRG1 (SWI/SNF-related, matrix-associated, actin-dependent regulator of chromatin, subfamily a, member 4) and other regulatory proteins such as *BACH1* (BTB and CNC homology 1, basic leucine zipper transcription factor 1) (36, 37). Indeed, chromatin modifier genes such as *BRD7* (bromodomain containing 7) *MLL2*, and *MLL3* (myeloid/lymphoid or mixed-lineage leukemia 2 and 3 were mutated in the PRCC2 samples (Table S1). This means that NRF2 activation in tumor cells or precancerous cells with malignant potential may lead to the activation of a different combination of genes than in normal cells, thus allowing identification of therapeutic targets unique to such cells.

Acknowledgements

We thank Sabrina Noyes for administrative support and David Nadziejka for technical editing.

References

1. Singh A, Misra V, Thimmulappa RK, Lee H, Ames S, Hoque MO, et al. Dysfunctional KEAP1-NRF2 interaction in non-small-cell lung cancer. PLoS Med. 2006;3:e420.

2. Shibata T, Kokubu A, Saito S, Narisawa-Saito M, Sasaki H, Aoyagi K, et al. NRF2 mutation confers malignant potential and resistance to chemoradiation therapy in advanced esophageal squamous cancer. Neoplasia. 2011;13:864-73.
3. Nioi P, Nguyen T. A mutation of Keap1 found in breast cancer impairs its ability to repress Nrf2 activity. Biochem Biophys Res Commun. 2007;362:816-21.
4. Tomlinson IP, Alam NA, Rowan AJ, Barclay E, Jaeger EE, Kelsell D, et al. Germline mutations in FH predispose to dominantly inherited uterine fibroids, skin leiomyomata and papillary renal cell cancer. Nat Genet. 2002;30:406-10.
5. Kinch L, Grishin NV, Brugarolas J. Succination of Keap1 and activation of Nrf2-dependent antioxidant pathways in FH-deficient papillary renal cell carcinoma type 2. Cancer Cell. 2011;20:418-20.
6. Ooi A, Wong JC, Petillo D, Roossien D, Perrier-Trudova V, Whitten D, et al. An antioxidant response phenotype shared between hereditary and sporadic type 2 papillary renal cell carcinoma. Cancer Cell. 2011;20:511-23.
7. http://picard.sourceforge.net.
8. Li H, Durbin R. Fast and accurate short read alignment with Burrows-Wheeler transform. Bioinformatics. 2009;25:1754-60.
9. Larson DE, Harris CC, Chen K, Koboldt DC, Abbott TE, Dooling DJ, et al. SomaticSniper: identification of somatic point mutations in whole genome sequencing data. Bioinformatics. 2012;28:311-7.
10. Trapnell C, Pachter L, Salzberg SL. TopHat: discovering splice junctions with RNA-Seq. Bioinformatics. 2009;25:1105-11.
11. Li H, Handsaker B, Wysoker A, Fennell T, Ruan J, Homer N, et al. The Sequence Alignment/Map format and SAMtools. Bioinformatics. 2009;25:2078-9.
12. Danecek P, Auton A, Abecasis G, Albers CA, Banks E, DePristo MA, et al. The variant call format and VCFtools. Bioinformatics. 2011;27:2156-8.
13. R-Development-Core-Team. R: A Language and Environment for Statistical Computing. 2011.
14. Urbanek S. multicore: Parallel processing of R code on machines with multiple cores or
CPUs. 2011.
15. Anders S, Huber W. Differential expression analysis for sequence count data. Genome Biol. 2010;11:R106.
16. Trapnell C, Roberts A, Goff L, Pertea G, Kim D, Kelley DR, et al. Differential gene and transcript expression analysis of RNA-seq experiments with TopHat and Cufflinks. Nat Protoc. 2012;7:562-78.
17. Benjamini Y, Hochberg Y. Controlling the False Discovery Rate: a Practical and Powerful Approach to Multiple Testing. J R Statist Soc B. 1995;57.
18. Furukawa M, Xiong Y. BTB protein Keap1 targets antioxidant transcription factor Nrf2 for ubiquitination by the Cullin 3-Roc1 ligase. Mol Cell Biol. 2005;25:162-71.
19. Brunet A, Sweeney LB, Sturgill JF, Chua KF, Greer PL, Lin Y, et al. Stress-dependent regulation of FOXO transcription factors by the SIRT1 deacetylase. Science. 2004;303:2011-5.
20. Stratton MR. Exploring the genomes of cancer cells: progress and promise. Science. 2011;331:1553-8.

21. McMahon M, Thomas N, Itoh K, Yamamoto M, Hayes JD. Redox-regulated turnover of Nrf2 is determined by at least two separate protein domains, the redox-sensitive Neh2 degron and the redox-insensitive Neh6 degron. J Biol Chem. 2004;279:31556-67.
22. Padmanabhan B, Tong KI, Ohta T, Nakamura Y, Scharlock M, Ohtsuji M, et al. Structural basis for defects of Keap1 activity provoked by its point mutations in lung cancer. Mol Cell. 2006;21:689-700.
23. Kobayashi A, Kang MI, Okawa H, Ohtsuji M, Zenke Y, Chiba T, et al. Oxidative stress sensor Keap1 functions as an adaptor for Cul3-based E3 ligase to regulate proteasomal degradation of Nrf2. Mol Cell Biol. 2004;24:7130-9.
24. Dinkova-Kostova AT, Holtzclaw WD, Cole RN, Itoh K, Wakabayashi N, Katoh Y, et al. Direct evidence that sulfhydryl groups of Keap1 are the sensors regulating induction of phase 2 enzymes that protect against carcinogens and oxidants. Proc Natl Acad Sci U S A. 2002;99:11908-13.
25. Kawai Y, Garduno L, Theodore M, Yang J, Arinze IJ. Acetylation-deacetylation of the transcription factor Nrf2 (nuclear factor erythroid 2-related factor 2) regulates its transcriptional activity and nucleocytoplasmic localization. J Biol Chem. 2011;286:7629-40.
26. Loignon M, Miao W, Hu L, Bier A, Bismar TA, Scrivens PJ, et al. Cul3 overexpression depletes Nrf2 in breast cancer and is associated with sensitivity to carcinogens, to oxidative stress, and to chemotherapy. Mol Cancer Ther. 2009;8:2432-40.
27. MacLeod AK, McMahon M, Plummer SM, Higgins LG, Penning TM, Igarashi K, et al. Characterization of the cancer chemopreventive NRF2-dependent gene battery in human keratinocytes: demonstration that the KEAP1-NRF2 pathway, and not the BACH1-NRF2 pathway, controls cytoprotection against electrophiles as well as redox-cycling compounds. Carcinogenesis. 2009;30:1571-80.
28. Venugopal R, Jaiswal AK. Nrf1 and Nrf2 positively and c-Fos and Fra1 negatively regulate the human antioxidant response element-mediated expression of NAD(P)H:quinone oxidoreductase1 gene. Proc Natl Acad Sci U S A. 1996;93:14960-5.
29. Reichard JF, Motz GT, Puga A. Heme oxygenase-1 induction by NRF2 requires inactivation of the transcriptional repressor BACH1. Nucleic Acids Res. 2007;35:7074-86.
30. Adam J, Hatipoglu E, O'Flaherty L, Ternette N, Sahgal N, Lockstone H, et al. Renal cyst formation in Fh1-deficient mice is independent of the Hif/Phd pathway: roles for fumarate in KEAP1 succination and Nrf2 signaling. Cancer Cell. 2011;20:524-37.
31. Ooi A, Furge KA. Fumarate hydratase inactivation in renal tumors: HIF1alpha, NRF2 and "cryptic targets" of transcription factors. Chin J Cancer. 2012.
32. DeNicola GM, Karreth FA, Humpton TJ, Gopinathan A, Wei C, Frese K, et al. Oncogene-induced Nrf2 transcription promotes ROS detoxification and tumorigenesis. Nature. 2011;475:106-9.
33. Shibata T, Saito S, Kokubu A, Suzuki T, Yamamoto M, Hirohashi S. Global downstream pathway analysis reveals a dependence of oncogenic NF-E2-related

factor 2 mutation on the mTOR growth signaling pathway. Cancer Res. 2010;70:9095-105.
34. Pearson KJ, Lewis KN, Price NL, Chang JW, Perez E, Cascajo MV, et al. Nrf2 mediates cancer protection but not prolongevity induced by caloric restriction. Proc Natl Acad Sci U S A. 2008;105:2325-30.
35. Kong AN, Yu R, Hebbar V, Chen C, Owuor E, Hu R, et al. Signal transduction events elicited by cancer prevention compounds. Mutat Res. 2001;480-481:231-41.
36. Zhang J, Ohta T, Maruyama A, Hosoya T, Nishikawa K, Maher JM, et al. BRG1 interacts with Nrf2 to selectively mediate HO-1 induction in response to oxidative stress. Mol Cell Biol. 2006;26:7942-52.
37. Sun J, Brand M, Zenke Y, Tashiro S, Groudine M, Igarashi K. Heme regulates the dynamic exchange of Bach1 and NF-E2-related factors in the Maf transcription factor network. Proc Natl Acad Sci U S A. 2004;101:1461-6.

Figure Legends

Figure 1. Somatic mutations to *NRF2*, *CUL3*, and *SIRT1* are found in sporadic PRCC2

The three-row rectangle in each panel is a heat map representing the read depth in the tumor sample (top row), the reference nucleotide sequence (hg18; center row), and the read depth in normal sequence (bottom row). Above and below the heat map, the percentage of mapped reads that differ from the reference genome are shown as bar charts, with the color of the bar representing the mutant nucleotide (grey represents deleted regions). The amino acid sequences in the tumor and normal samples are shown, respectively, above and below the bar charts. **A**. Case-831, *NRF2* c.245A>G mutation, resulting in an E82G amino acid change. **B**. Case-666, *SIRT1* c.808T>C mutation, resulting in I270T amino acid change, and *NRF2* c.105_107delGTA, resulting in deletion of valine 36. **C**. Case-337, *CUL3* c.1168delT resulting in a frame-shift (L390fs). **D**. Case-790, *CUL3* c.2125C>T mutation, resulting in R708W amino acid change.

Figure 2. Effect of gene mutations on NRF2 transcriptional activity as measured by luciferase reporter assay in PCS-400 cells. **A**. The expression of KEAP1 lowered the transcription activity of wild-type NRF2 but not of the E82G mutant, indicating the mutant's resistance toward KEAP1-mediated regulation. The expression of HA-KEAP1 was followed on western blot (lower panel) using an antibody against the human influenza hemagglutinin (HA) tag, while NRF2 activity is followed using luciferase assay; a Relative Luminescence Unit (RLU) was the read-out of NRF2 activity. **B**. The V36del NRF2 mutant was more resistant to KEAP1-mediated regulation than wild-type NRF2, and the expression of the I270T SIRT1 mutant further increased its activity. Expression of both wild-type and mutant SIRT1 were followed on western blot using an antibody against Flag-Tag (F-SIRT1, lower panel); the expression of HA-KEAP1 was followed as in panel "**A**". **C**. Two different species of siRNA were used in independent experiments to knockdown CUL3 in PCS-400 cells, and both achieved reasonable knockdown of CUL3 protein level (lower panel). This reduction in CUL3 resulted in increased NRF2 activity, suggesting that a CUL3 loss-of-function mutation can cause NRF2 activation.

Figure 3. Transcriptome sequencing revealed up-regulation of NRF2 transcription targets and immunostaining confirmed NRF2 activation. **A**. Changes in the transcript level of transcription targets of NRF2. Each row on the heat map represents individual exons of the indicated genes. Each column represents an individual sample, either normal kidney tissue (N) or tumor tissue (T). The transcript level of these genes was higher in the tumor tissues, suggesting increased NRF2 activity. **B**.

Immunohistochemical staining of NRF2 in the 5 cases PRCC2, scale bar = 0.1 mm. **C**. Immunohistochemical staining of NRF2 in normal kidney tissue; scale bar = 0.1 mm. **D**. Immunohistochemical staining of NRF2 in two cases of clear cell renal cell carcinoma randomly selected for this study; scale bar = 0.1 mm.

Figure 4. Transcriptome sequencing revealed the expression pattern of the mutant alleles.

Stacked bar plots showing the expression of mutant alleles in tumors (T) and normal (N) tissues; left y-axis (black) shows the number of reads, and the right y-axis (blue) shows the FPKM value. Each bar shows a single nucleotide at the specified location. The blue dot on the plot shows the median FPKM value, and the error bar indicates the upper and lower FPKM values. Individual nucleotide species are color-coded; grey represents a deletion. The genomic locations of the mutation are indicated at the bottom of each plot. **A**. Case-831, *NRF2* c.245A>G. **B**. Case-666, *NRF2* c.105_107delGTA and *SIRT1* c.808T>C mutations. **C**. Case-790, *CUL3* c.2125C>T mutation. **D**. Case-337, *CUL3* c.1168delT transcript is not present in the transcriptome.

Figure 1

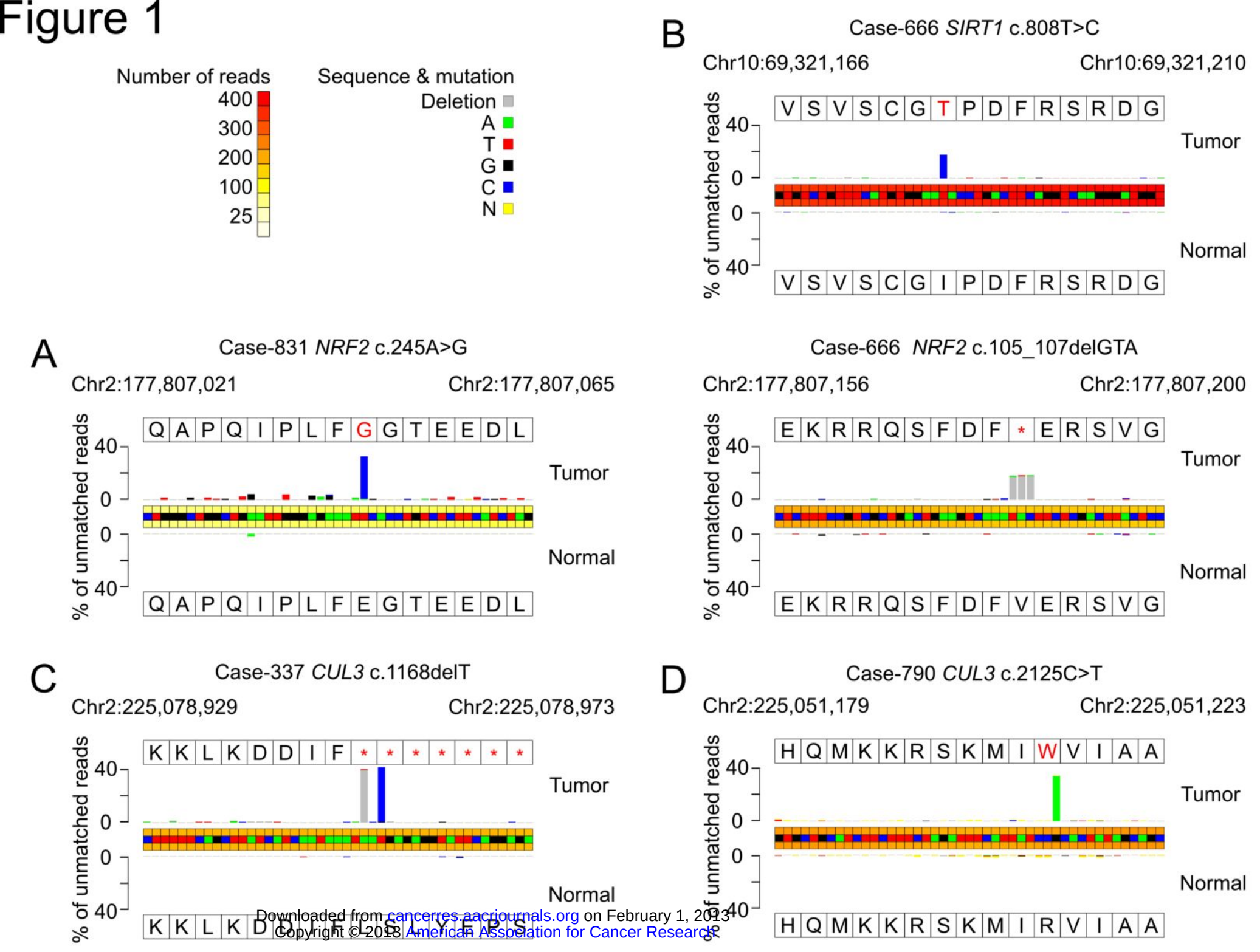

Figure 2

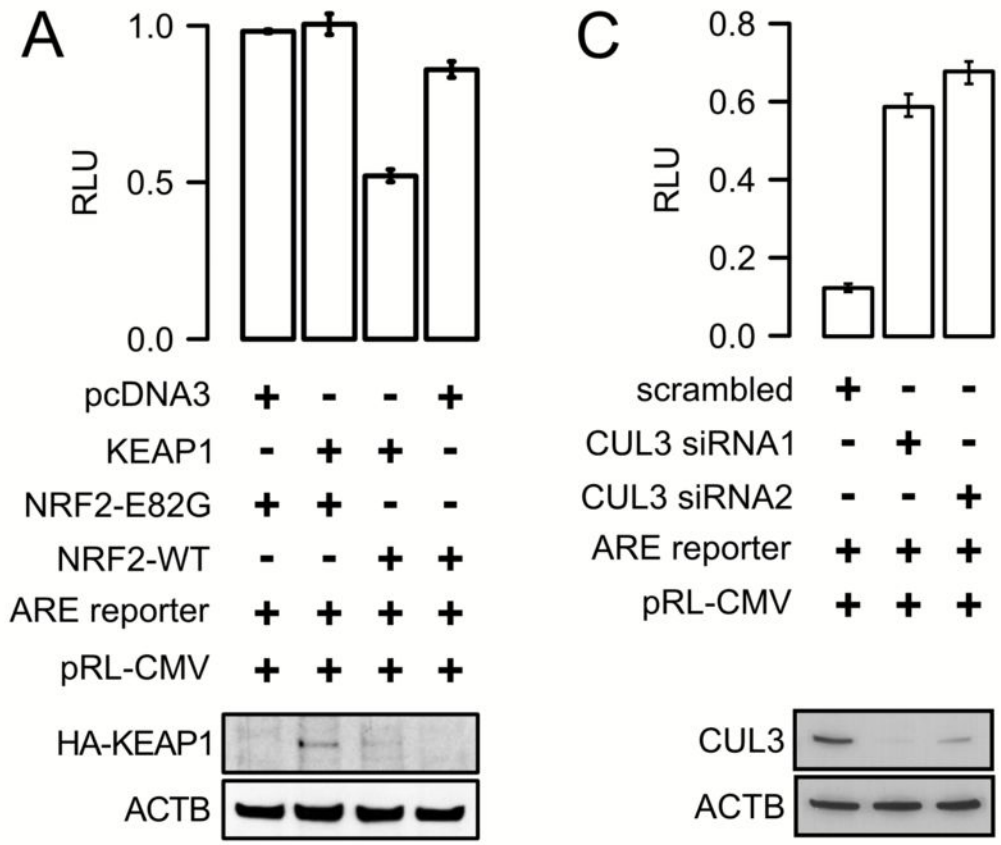

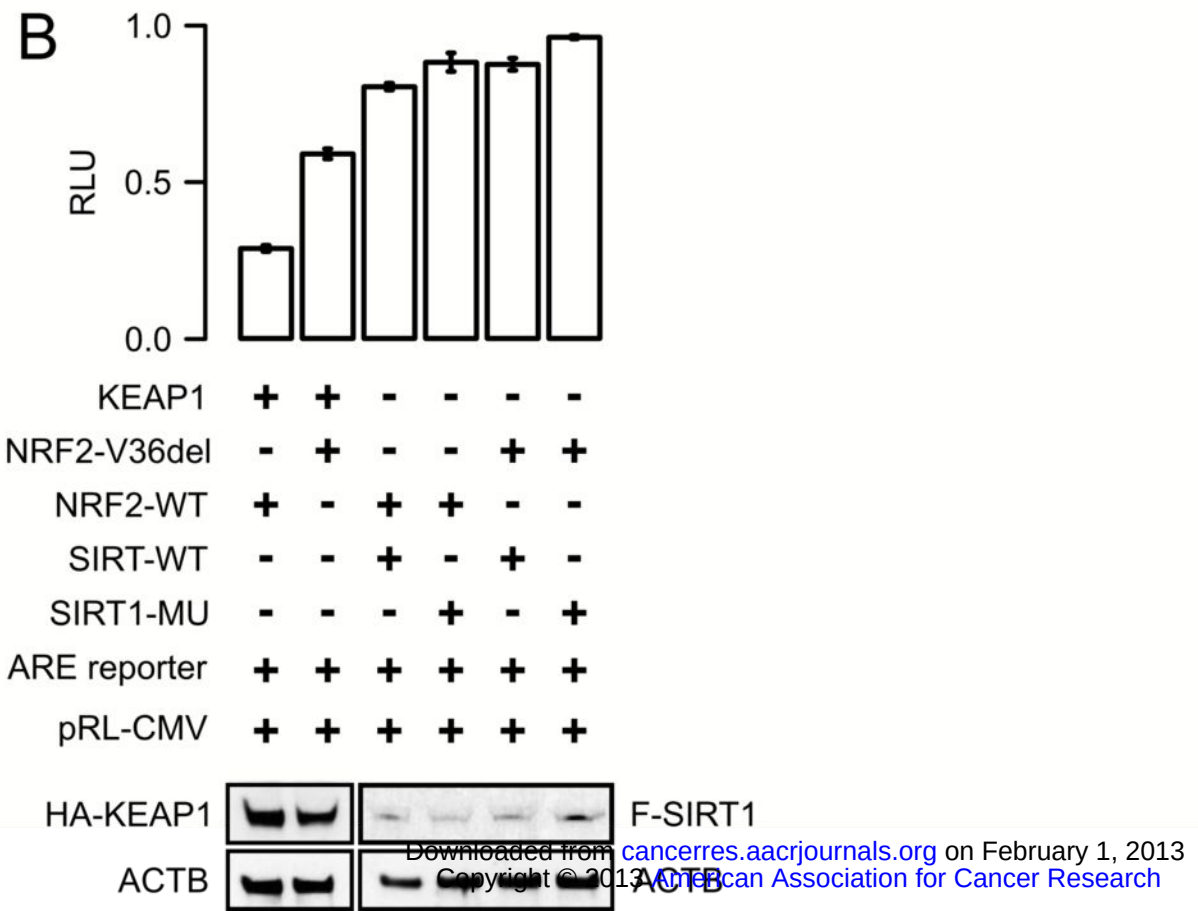

Figure 3

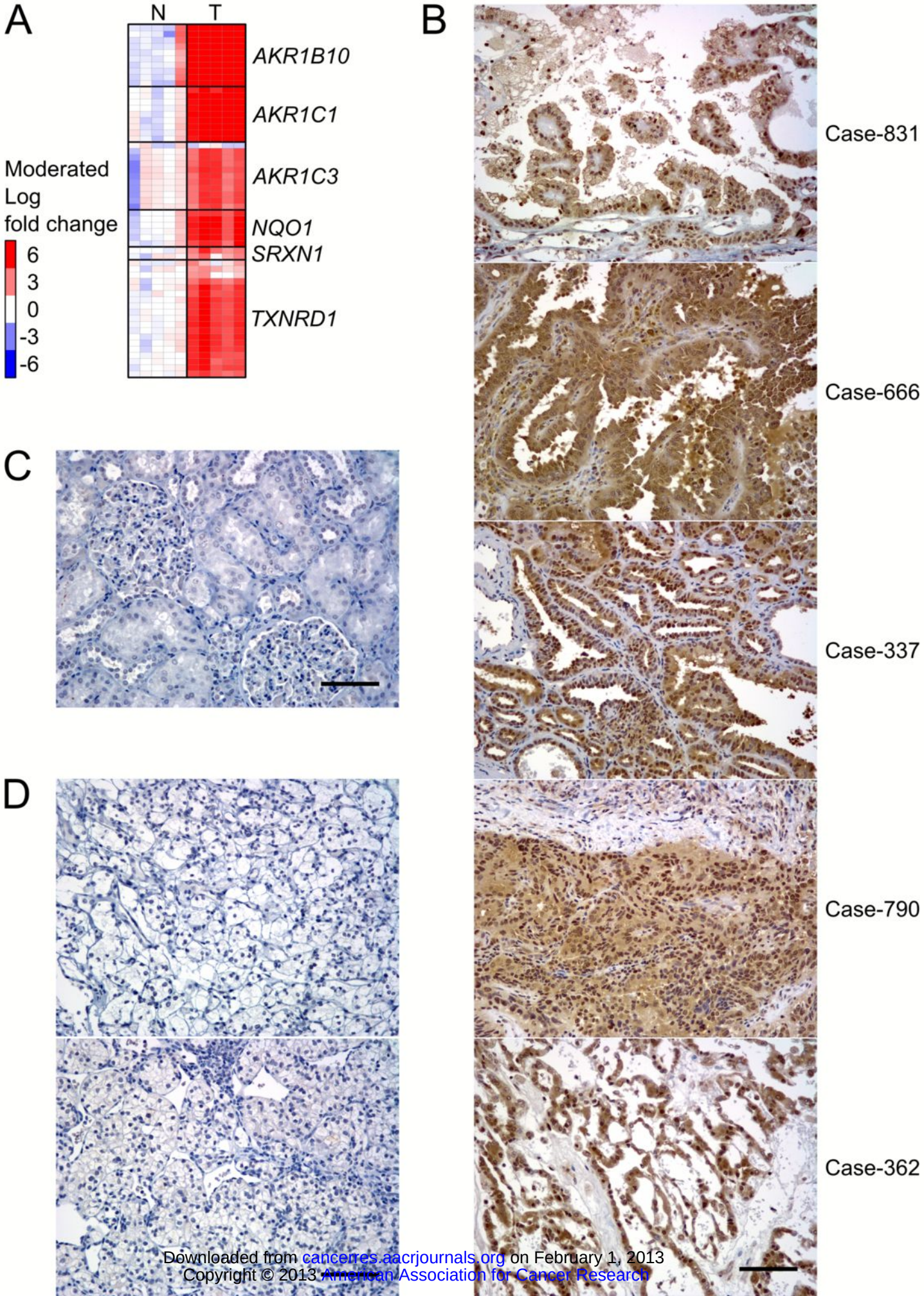

Figure 4